PREPARATION AND PROPERTIES OF $Sr_3B_2O_6:Dy^{3+},Eu^{3+}$ WHITE PHOSPHORS USING HIGH TEMPERATURE SOLID-STATE METHOD**

Y. Li [1*], W. H. Shi [1], L. M. Dong [2], S. X. Xu [1], H. J. Huang [1], J. R. Yin [1]

[1] Guangxi Key Laboratory of Optical and Electronic Materials and Devices, Guilin University of Technology, Guilin, China; e-mail: liyou@glut.edu.cn
[2] Key Laboratory of Engineering Dielectrics and Its Application, Ministry of Education, Harbin University of Science and Technology, Harbin, China

$Sr_3B_2O_6:Dy^{3+},Eu^{3+}$ single-matrix white-light-emitting materials are prepared using the high-temperature solid-state method. The microstructure, emission spectrum, energy transfer mechanism, and color brightness of the samples are studied using scanning electron microscopy, X-ray diffraction, fluorescence spectrophotometry, and color coordinate (CIE) calculations. Furthermore, the effects of the synthesis temperature, holding time, rare-earth element doping amount, and charge compensation agent on the luminescence intensity of the samples are investigated. Results show that the luminescent effect of the sample containing Na^+ as the charge compensator is better than that of the sample containing K^+. When the concentrations of Dy^{3+} and Eu^{3+} are 2 and 3%, respectively, the calcination temperature is 700°C, and the holding time is 3 h, the samples exhibit the best luminescence performance and the color coordinates are in the white-light region, indicating a good white-light luminescent material.

Keywords: *borate, high temperature solid-state method, emission spectrum, luminescent material.*

ОПТИЧЕСКИЕ СВОЙСТВА БЕЛЫХ ЛЮМИНОФОРОВ $Sr_3B_2O_6:Dy^{3+},Eu^{3+}$, СИНТЕЗИРОВАННЫХ ВЫСОКОТЕМПЕРАТУРНЫМ ТВЕРДОФАЗНЫМ МЕТОДОМ

Y. Li [1*], W. H. Shi [1], L. M. Dong [2], S. X. Xu [1], H. J. Huang [1], J. R. Yin [1]

УДК 535.37

[1] Гуйлиньский технологический университет, Гуйлинь, Китай; e-mail: liyou@glut.edu.cn
[2] Харбинский университет науки и технологий, Харбин, Китай

(Поступила 9 июня 2021)

Высокотемпературным твердофазным методом получены одноматричные светоизлучающие материалы $Sr_3B_2O_6:Dy^{3+},Eu^{3+}$. Микроструктура, спектр излучения, механизм переноса энергии и цветовая яркость образцов изучены с помощью сканирующей электронной микроскопии, рентгеноструктурного анализа, флуоресцентной спектрофотометрии и расчетов цветовых координат. Исследовано влияние температуры синтеза, времени выдержки, количества легирующих редкоземельных элементов и агента компенсации заряда на интенсивность люминесценции образцов. Показано, что люминесцентные свойства образца, содержащего Na^+ в качестве компенсатора заряда, лучше свойств образца, содержащего K^+. При содержании Dy^{3+} и Eu^{3+} 2 и 3 %, температуре прокаливания 700 °C и времени выдержки 3 ч образцы проявляют наилучшие люминесцентные характеристики, а координаты цвета находятся в белом свете.

Ключевые слова: *борат, высокотемпературный твердотельный метод, спектр излучения, люминесцентный материал.*

**Full text is published in JAS V. 89, No. 3 (http://springer.com/journal/10812) and in electronic version of ZhPS V. 89, No. 3 (http://www.elibrary.ru/title_about.asp?id=7318; sales@elibrary.ru).

Introduction. With the continuous development of the light-emitting diode (LED) industry, extensive research is being performed on fluorescent materials. Phosphors have been widely used for single-matrix white LEDs owing to their good performance [1]. Currently, there are two main methods for obtaining white LEDs: the red–green–blue tricolor-chip-composite method and the phosphor conversion method. The phosphor conversion method is favored because of its low cost and simple integration process. Using this method, white light can be obtained by combining blue light emitted by a blue chip and yellow light emitted by phosphor. A single-matrix trichromatic phosphor or broad-spectrum phosphor can also be coated on the ultraviolet (UV) chip to obtain white light by trichromatic recombination [2–4]. However, when tricolor phosphors are mixed to obtain white-light emissions, they suffer from color reabsorption and ratio regulation, which considerably affect the lumen efficiency and color reducibility of the prepared LED. The use of UV and near-UV chips to excite tricolor white phosphor to achieve white-light emissions is a good alternative [5–7].

Recently, the physicochemical properties of rare-earth elements have been widely favored for preparing white LEDs [8]. The required properties can be achieved by doping different ions, and the commonly used ions are Dy^{3+} [9], Mn^{2+} [10], Tb^{3+} [11], and Eu^{3+} [12]. The phosphor matrix currently used for white LEDs mainly includes aluminates [13], sulfides [14], silicates [15], borates [16], and nitrides [17]. Borate-based luminescent materials are considered one of the most practical luminescent materials because of their low calcination temperature, high-luminescence brightness, and good chemical stability, because of which they have always been a research hotspot [18–21]. Wang et al. [22] synthesized $Sr_3B_2O_6:Eu^{3+}$, Na^+ phosphors that can be used in white LEDs using the high-temperature solid-state method and studied the effects of the calcination time, rare-earth element (Eu^{3+}) doping amount, and other conditions on the luminescent properties of the material. Lin et al. [23] synthesized Dy^{3+}-doped $Sr_3B_2O_6$ phosphor for obtaining white light and they studied the phase purity, luminescence performance, and chromaticity coordinate position of the prepared phosphor. Moreover, Ce^{3+} and Eu^{2+} double-doped $Sr_3B_2O_6$ phosphors have been reported [24]. Chang et al. [25] prepared Ce^{3+} and Eu^{2+} double-doped single-matrix white-light $Sr_3B_2O_6$ phosphors for UV LED excitation using the high-temperature solid-state method and they studied the energy transfer process of Ce^{3+} and Eu^{2+}. However, there are limited explanations about the effects of the rare-earth element doping amount and charge compensation agent on $Sr_3B_2O_6:Dy^{3+}$, Eu^{3+} single-matrix white phosphors.

In this study, $Sr_3B_2O_6:Dy^{3+}$, Eu^{3+} single-matrix white phosphors were prepared using the high-temperature solid-state method. Moreover, the properties of the luminescent materials were investigated and the effects of the synthesis temperature, holding time, charge compensation agent, and rare-earth element doping amount on the luminescent properties of the samples were theoretically analyzed and studied in detail.

Experimental. Using the high-temperature solid-state method, the mass of H_3BO_3, Eu_2O_3, Na_2CO_3, Dy_2O_3, K_2CO_3, and $SrCO_3$ for sample preparation according to the stoichiometric ratio was calculated. Then, these compounds were added to a mortar and ground for 1 h to obtain an even mixture. Next, the mixture was placed into a crucible and the crucible was placed in a resistance furnace, where the temperature (650, 700, 750, 800, 850, and 900°C) and holding time (2, 3, 4, 5, and 6 h) were set for preburning. The preburned samples were removed from the furnace, ground, and then placed back into the high-temperature resistance furnace for calcination. After calcination, the samples were cooled to room temperature in the furnace and then removed. After sufficient grinding for 2 h, the required powder samples were obtained.

An X-ray diffraction (XRD) analyzer (HT100, American Elite Technology Co., Ltd.) was used to analyze the phase and morphology of the samples. Field emission scanning electron microscopy (FE-SEM. Sirion-200, Phillips) was used to analyze the microstructure of the phosphor. The working voltage of the scanning electron microscope was set to 20 kV. The excitation and emission spectra of the samples were measured using an RF-5301 fluorescence spectrophotometer.

Results and discussion. *Structure and fluorescence properties of luminescent materials.* Figure 1 shows a comparison between the XRD patterns of $Sr_3B_2O_6:Eu^{3+}$, Dy^{3+} at 700°C and a holding time of 3 h and the standard XRD patterns of $Sr_3B_2O_6$. The SEM image of the $Sr_3B_2O_6:Eu^{3+}$, Dy^{3+} samples prepared at 700°C for 4 h is presented. When the synthesis temperature and holding time are 700°C and 3 h, respectively, the XRD patterns of $Sr_3B_2O_6:Eu^{3+}$, Dy^{3+} are consistent with the standard XRD patterns of $Sr_3B_2O_6$. This indicates that the experimentally obtained sample corresponds to the $Sr_3B_2O_6$ phase, and the addition of a small amount of Eu^{3+} and Dy^{3+} does not affect the crystal structure. Only two low-intensity peaks are detected, corresponding to the impurities of $Eu_2(CO_3)_3$ produced in the reaction process. The illustration reveals a uniform granular surface morphology of the phosphor sample with nonsmooth particle surfaces; however, the interface is clear. The radii of the particles are 0.5–1 μm, and the particles are locally adhered.

The small size and uniformity of the phosphor particles can improve the coating performance of the phosphor, facilitating a uniform emission.

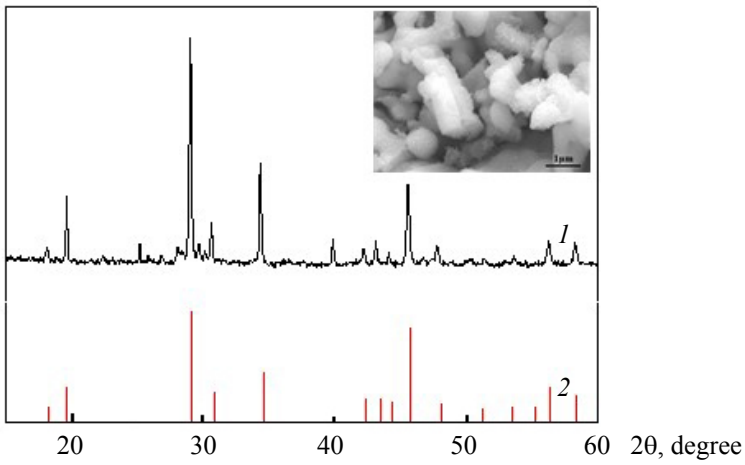

Fig. 1. The comparison between (1) the XRD patterns of $Sr_3B_2O_6:Eu^{3+}$, Dy^{3+} under the holding time of 3 h at 700°C and (2) the standard XRD patterns of $Sr_3B_2O_6$. The illustration is an SEM image of $Sr_3B_2O_6:Eu^{3+}$, Dy^{3+} synthesis at 700°C for 4 h.

Figure 2 shows the excitation and emission spectra of $Sr_3B_2O_6:Eu^{3+}$, Dy^{3+}; the illustration presents the color coordinate (CIE) diagram of $Sr_3B_2O_6:Dy^{3+}$, Eu^{3+}. The excitation spectrum of the sample comprises wide absorption bands and some sharp peaks. The 4f–4f transition absorption peak of Eu^{3+} is observed at 393 nm, while the energy levels of Dy^{3+} are $^6H_{15/2}$–$^6P_{2/3}$, $^6H_{15/2}$–$^6P_{2/7}$, $^6H_{15/2}$–$^6P_{2/5}$, and $^6H_{15/2}$–$^6M_{21/2}$, corresponding to the absorption peaks at 320, 349, 363, and 385 nm, respectively. The asymmetric peak at 380–400 nm is ascribed to the superposition of the absorption peaks of Eu^{3+} and Dy^{3+}; the absorption and emission peaks of Eu^{3+} and Dy^{3+} are not simply superimposed, the two ions will affect each other and undergo energy transfer simultaneously. The excitation peak reveals that the prepared luminescent material can be used for the excitation of near-UV light and blue-light chips.

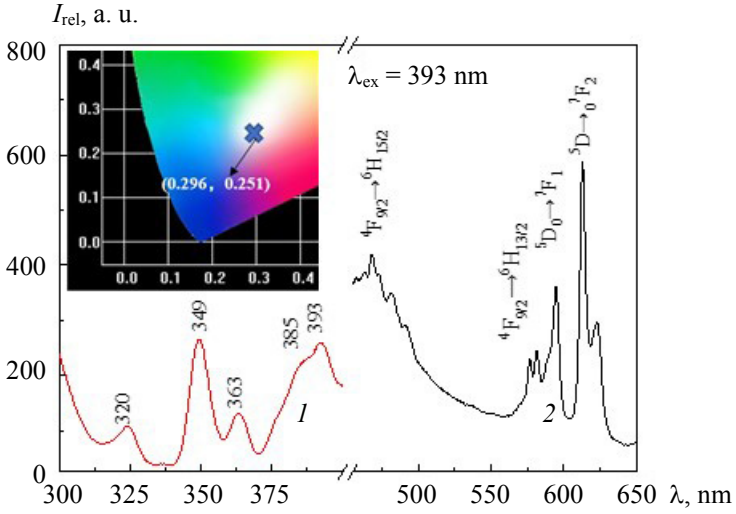

Fig. 2. Excitation (1) and emission (2) spectra of $Sr_3B_2O_6:Eu^{3+}$, Dy^{3+} phosphor. The illustration is the CIE pattern of $Sr_3B_2O_6:Dy^{3+}$, Eu^{3+}.

Furthermore, sharp peaks are detected at 590 and 612 nm, representing the characteristic emission peaks of $^5D_0$–^7F_J (J = 1, 2, 3, 4) of Eu^{3+}. The magnetic dipole transition is dominant, emitting yellow-orange light at 590 nm. When the *f–f* forbidden transition is partially stopped, an electric dipole transition of $^5D_0$–$^7F_2$ appears, emitting red light at 610 nm. This transition helps improve the luminescence performance of the phosphor. Moreover, the intensity of the electric dipole transition from $^5D_0$–$^7F_2$ is higher than that of the magnetic dipole transition from $^5D_0$–$^7F_1$, which is caused by the difference in the numbers of the two light-emitting centers. Dy^{3+} luminescence is attributed to two emission peaks in the visible light range. The center values are achieved at 472 and 575 nm, corresponding to $^4F_{9/2}$–$^6H_{15/2}$ and $^4F_{9/2}$–$^6H_{13/2}$ transitions, respectively. With the addition of Eu^{3+}, the emission peak corresponding to $^4F_{9/2}$–$^6H_{13/2}$ at 575 nm becomes weaker because of the increase in the number of luminescence centers and decrease in the luminescence intermediate distance. The illustration shows that white light can be obtained by adding an appropriate amount of Eu^{3+}, and the color coordinates at this time are X = 0.296 and Y = 0.251.

Study of the calcination process. Figure 3 presents the emission intensity of $Sr_3B_2O_6$:Dy^{3+} calcined at 650, 700, 750, 800, 850, and 900°C for 3 h. This figure shows that when the calcination temperature is 650°C, the intensity of the emission spectrum is very low, indicating that the crystallinity of $Sr_3B_2O_6$ cannot be improved at this temperature. Most of the Dy^{3+} does not enter the crystal lattice to occupy cation vacancies and form a luminescent center; thus, the phosphor is not fired. When the synthesis temperature increases to 700°C, the relative intensity displayed on the spectrum is the highest. As the synthesis temperature continues to increase, the intensity decreases. This is because as the calcination temperature increases, the grains continue to grow and the samples agglomerate, thus decreasing the luminescence intensity of the samples. The morphology of the phosphor has a great influence on its luminescence performance and coating performance in an LED package; thus, 700°C is the ideal temperature.

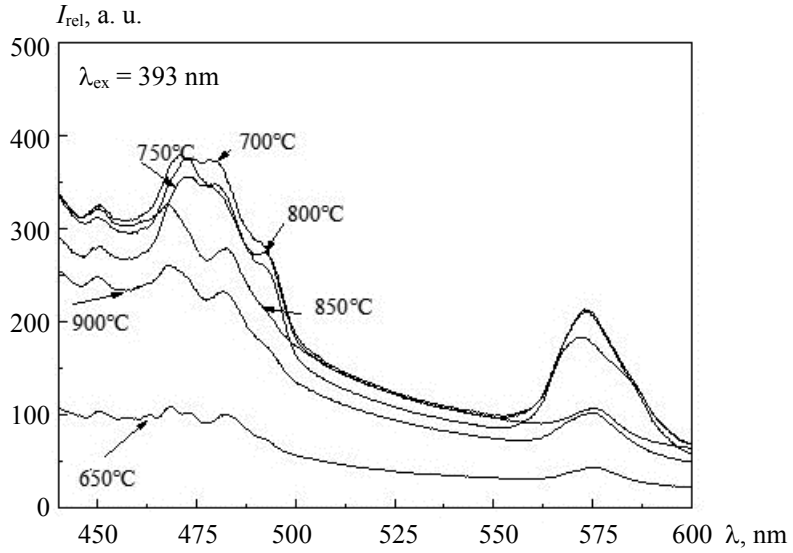

Fig. 3. Emission intensity diagram of $Sr_3B_2O_6$: Dy^{3+} calcined at 650, 700, 750, 800, 850, and 900°C for 3 h.

Figure 4 shows the SEM images of $Sr_3B_2O_6$:Dy^{3+} calcined at different temperatures for 3 h. This figure reveals that only a small part of the samples crystallizes at 650°C because this temperature is too low to maintain the energy required during the calcination process. The calcination effect of the sample is better at 700°C than at 650°C because the surface morphology of phosphor consists of relatively uniform granular particles, the particle surface is smoother, and the interface is clear. The particle diameters are approximately 0.5–1.0 μm. The sample with this morphology has good coating performance and uniform luminescence. When the synthesis temperature increases to 750°C, the particle dispersion of the sample decreases, the agglomeration phenomenon begins to appear, and the particle size is nonuniform. As the synthesis temperature continues to increase, the particle dispersion decreases sharply. At 800°C, the agglomeration phenomenon is obvious.

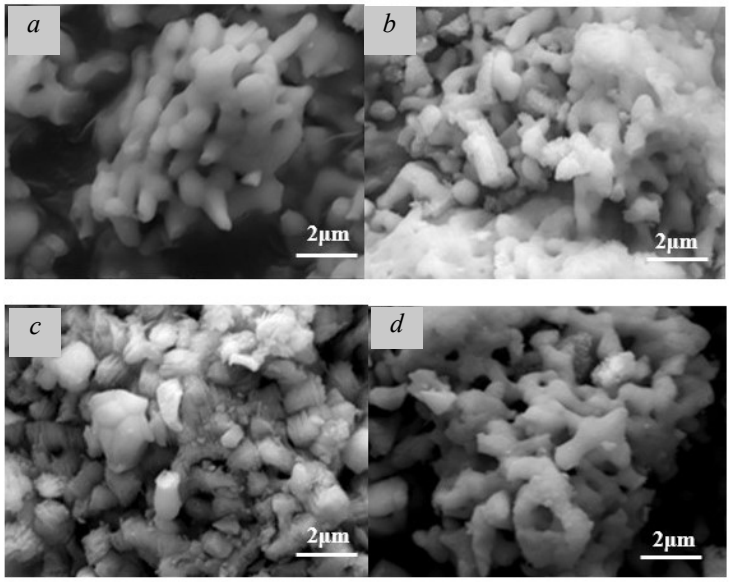

Fig. 4. The SEM patterns of $Sr_3B_2O_6:Dy^{3+}$ calcined at temperatures 650 (a), 700 (b), 750 (c), and 800°C (d) for 3 h.

Figure 5 shows the emission spectra of $Sr_3B_2O_6:Dy^{3+}$ under different holding times at 700°C. The holding time has a considerable influence on the luminescence performance of the sample. An appropriate holding time can promote the diffusion of ions in the raw materials, which is conducive for the growth of crystals; furthermore, it can improve the luminescence performance of phosphors. If the holding time is excessively long, the crystals undergo excess growth and the subsequent crushing process yields a new surface. After being packaged in the LED, the phosphor becomes unstable, which shortens its service life. The high-temperature solid-state method for preparing phosphors does not include the step regarding uniform mixing of raw materials in the liquid phase, and the diffusion of ions during the formation of crystal lattices is obstructed. Therefore, the holding time must be adjusted so that the rare-earth elements can successfully enter the crystal lattice without causing an excess growth of crystals. Figure 5 shows that 3 h is the most suitable holding time.

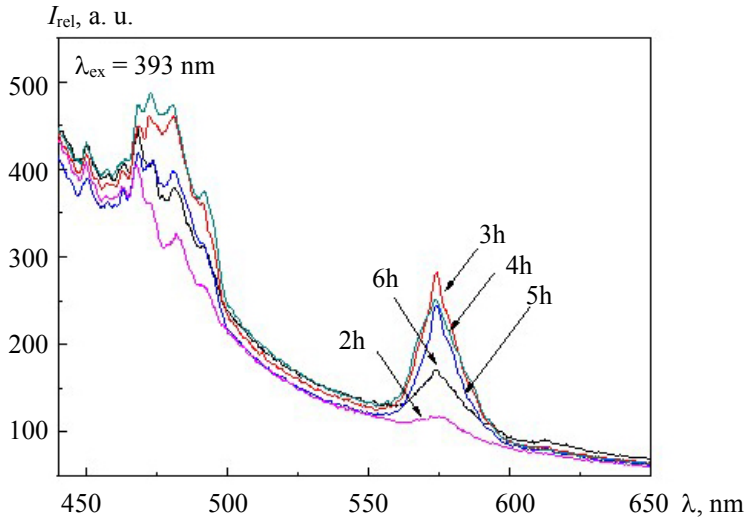

Fig. 5. Emission intensity of $Sr_3B_2O_6:Dy^{3+}$ under different holding times (2, 3, 4, 5, and 6 h) at 700°C.

Figure 6 shows the XRD patterns of $Sr_3B_2O_6:Dy^{3+}$ under different holding times at 700°C. When the holding time is 2 h, the XRD pattern shows an obvious miscellaneous peak, which is a characteristic peak of the crystal phase of europium carbonate. When the holding time increases to 3 h, the characteristic peak of

europium carbonate decreases. As the holding time continues to increase, the characteristic peak intensity of europium carbonate changes slightly, showing only slight enhancements. This is caused by the decomposition of europium carbonate on the crystal lattice surface. With the prolongation of time past 3 h, the reaction of europium carbonate on the crystal lattice surface is complete; furthermore, the rare-earth ions gradually undergo even diffusion. Some rare-earth ions diffuse on the crystal lattice surface to form europium carbonate, and the characteristic peak intensity of europium carbonate changes slightly. Therefore, considering the crystallization and luminescence properties of the reaction product as well as energy- and cost-saving aspects, 3-h calcination is more suitable than the other tested holding times.

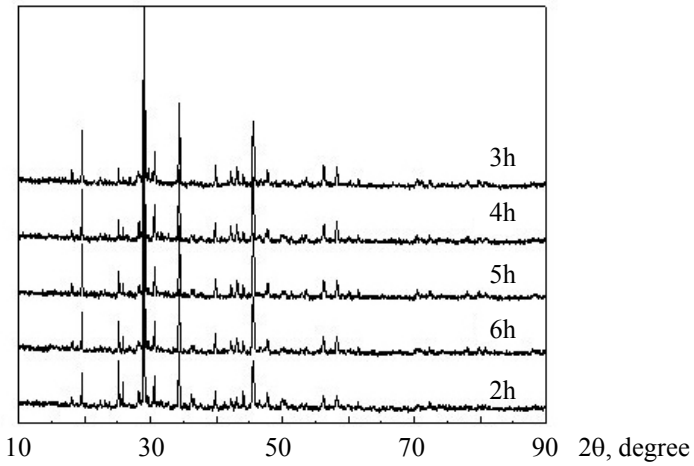

Fig. 6. The XRD patterns of $Sr_3B_2O_6:Dy^{3+}$ under different holding times (2, 3, 4, 5, and 6 h) at 700°C.

Research on the influence of doping elements on luminescence performance. Figure 7 shows the effect of the charge compensator on the luminescence properties of $Sr_3B_2O_6:Dy^{3+}$, Eu^{3+}. The luminescence intensity of the sample with a charge compensator is higher than that of the sample without a charge compensator, indicating that the charge compensator is instrumental in $Sr_3B_2O_6$. The luminescence effect of the sample containing Na^+ as a charge compensator is better than that of the sample containing K^+. The calculation shows that the radii of Sr, Na, and K are 0.219, 0.190, and 0.243 nm, respectively. Compared with K^+, the radii of Na^+ and Sr^{2+} are closer in size, and Na^+ and Sr^{2+} enter the crystal lattice more easily; hence, the probability of lattice distortion is smaller. Therefore, Na^+ can replace Sr^{2+} to produce a charge compensation effect and increase the sample luminescence intensity. Figure 7 shows that at 610 nm, the emission peak intensity of the sample containing Na^+ as the charge compensator is 282% higher than that of the sample without Na^+.

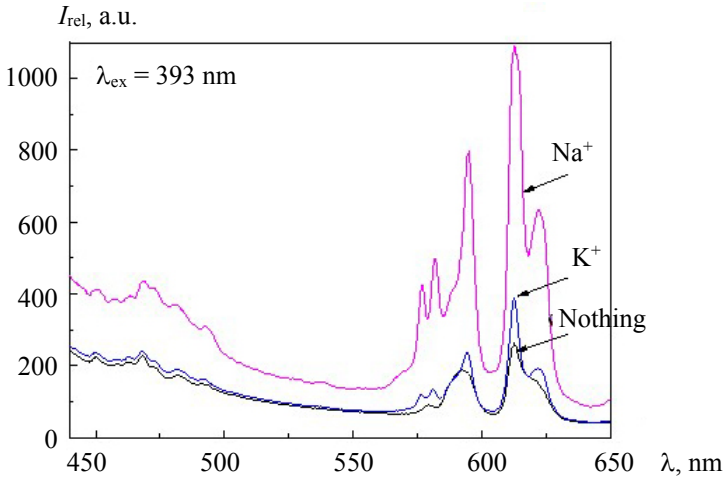

Fig. 7. Emission spectra of $Sr_3B_2O_6:Eu^{3+}$, Dy^{3+} with and without Na^+ or K^+.

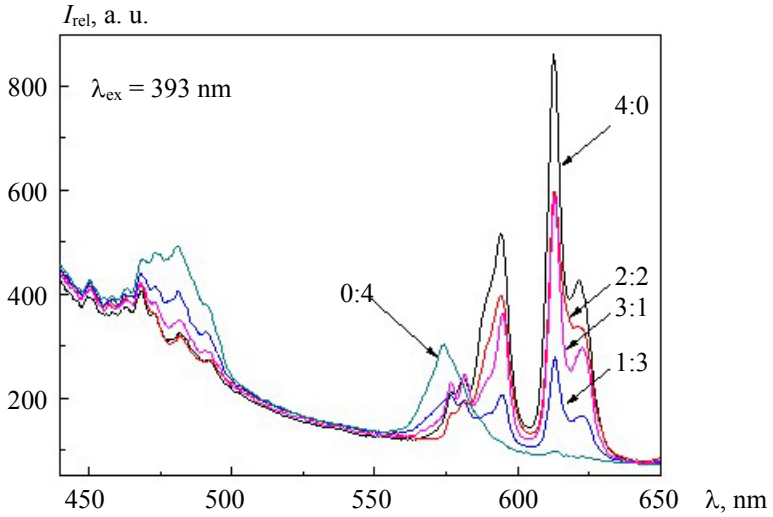

Fig. 8. Emission intensity of $Sr_3B_2O_6:Eu^{3+}$, Dy^{3+} in different doping concentrations (0:4%, 1:3%, 2:2%, 3:1%, 4:0%) of Eu^{3+}, Dy^{3+}.

Figure 8 depicts the emission spectra of different Eu^{3+} and Dy^{3+} concentrations of $Sr_3B_2O_6:Eu^{3+}$, Dy^{3+} phosphors. When the doping ion is only Dy^{3+}, the luminescence region is observed in the blue-and yellow-light bands. The yellow-light emission intensity is lower than the blue-light emission intensity; hence, the color temperature is very high and the color is bluish without white light. When the doping ion is only Eu^{3+}, the luminescence region is detected in the orange- and red-light bands and no white light is observed. However, the superposition of the emission spectra of the two ions can yield warm white light. The $^4F_{9/2}$–$^6H_{13/2}$ transition of Dy^{3+} is very sensitive at 575 nm. Figure 8 shows that the peak intensity at 575 nm decreases with the addition of Eu^{3+}; however, with increasing doping concentrations, the peak intensity tends to stabilize at a constant value. When the concentration of each Eu^{3+} and Dy^{3+} is 2%, the luminescence intensity of the two ions is the highest. Hence, the Dy^{3+} concentration was set at 2% and the Eu^{3+} concentration was changed to adjust the color coordinates of the phosphor.

Figure 9 depicts the emission spectra of $Sr_3B_2O_6$: Eu^{3+}, Dy^{3+} phosphors at different Eu^{3+} doping concentrations when the Dy^{3+} concentration is 2%. The illustration shows the color coordinates of $Sr_3B_2O_6:Eu^{3+}$, Dy^{3+} phosphors at different Eu^{3+} doping concentrations. The Eu^{3+} doping concentration only affects the orange and red luminescence intensities of the phosphors and has no effect on the position of the emission

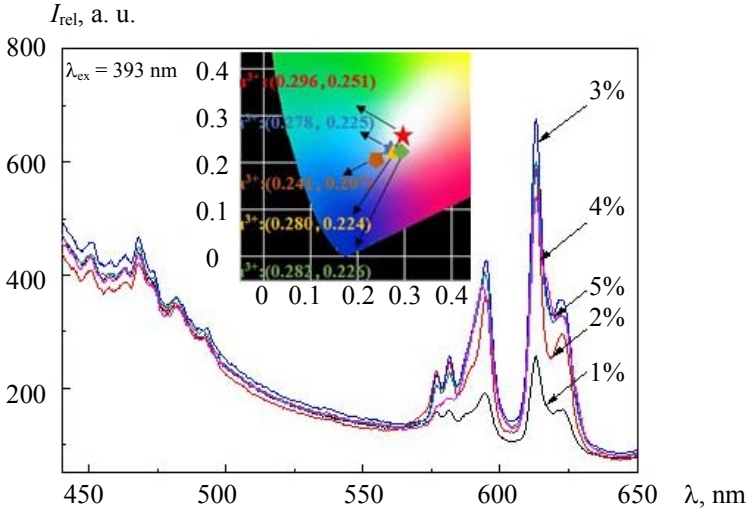

Fig. 9. Emission intensity of $Sr_3B_2O_6:Eu^{3+}$, Dy^{3+} in different doping concentrations (1, 2, 3, 4, and 5%) of Eu^{3+}.

peak. When the Eu^{3+} concentration is small, the emission centers are isolated owing to limited red emission centers and the total energy transferred between the emission centers is small. With an increase in the Eu^{3+} concentration, the orange light gradually increases. White light can be produced when a small amount of yellow light is mixed with orange, red, and blue lights excited by Dy^{3+}, and the emission color coordinate is at the white-light position. When the Eu^{3+} concentration is 3%, the luminescence intensity reaches the maximum value. The color coordinate diagram reveals that under the condition of a constant Dy^{3+} ion concentration, the light-emitting area shows a red shift as the Eu^{3+} concentration increases, and the mixture of blue and yellow-orange light can produce white light under near-UV excitation. Based on the color coordinate diagram, when the concentrations of Dy^{3+} and Eu^{3+} are 2 and 3%, respectively, the color coordinates of the emission spectrum are closest to the center of the white-light region. The illustration is of the CIE pattern of $Sr_3B_2O_6$:Dy^{3+}, Eu^{3+} at different Eu^{3+} doping concentrations.

Conclusions. $Sr_3B_2O_6$:Eu^{3+}, Dy^{3+} phosphors are prepared using the high-temperature solid-state method. The best sintering condition is a temperature of 700°C maintained for 3 h. When $Sr_3B_2O_6$:Dy^{3+}, Eu^{3+} is synthesized at this temperature and holding time, with doping concentrations of 2% Dy^{3+} and 3% Eu^{3+}, the color coordinates of the emission spectrum are closest to the center of the white-light region and the luminescence performance is the best of all the samples tested in this work. A comparison of the emission peak at 610 nm between samples, with and without Na^+ as the charge compensator, indicates that the emission peak intensity increases by 282%. Therefore, $Sr_3B_2O_6$:Eu^{3+}, Dy^{3+} can achieve good fluorescence performance and be used as a single-matrix white light-emitting material for LEDs excited using near UV or blue light.

Acknowledgements. This work was supported by the Guangxi Base and Talents Project (AD19110086), the Foundation of Guilin University of Technology (GUTQDJJ2018024), and the Open Foundation, Guangxi Key Laboratory of Optical and Electronic Materials and Devices (20KF-14).

REFERENCES

1. Y. Xie, Y. Yin, R. X. Zhang, H. B. Wang, *New. Chem. Mater*., **40**, No. 2, 24–27 (2012).
2. Q. Su, H. Wu, Y. X. Pan, C. F. Guo, *J. Rare Earths*., **23**, No. 5, 513–517 (2005).
3. L. Kong, S. C. Gan, G. Y. Hong, J. L. Zhang, *Chin. J. Lumin*., **28**, No. 3, 393–396 (2007).
4. Q. S. Liu, X. Y. Hao, G. F. Xu, L. Zhao, D. D Cao, *Chin. J. Inorg. Chem*., **26**, No. 7, 1303–1306 (2010).
5. S. Pimputkar, J. S. Speck, S. P. DenBaars, S. Nakamura, *Nat. Photon*., **3**, 180–182 (2009).
6. W. Y. He, Wang X. F. Wang, J. Zheng, X. H. Yan, *J. Am. Ceram. Soc*., **97**, No. 6, 1750–1755 (2014).
7. W. Lv, Y. C. Jia, Q. Zhao, W. Z. Lv, H. P. You, *Chem. Commun*., **50**, No. 20, 2635–2637 (2014).
8. H. X. Liu, Z. Y. Guo, *J. Lumin*., **187**, 181–185 (2017).
9. R. L. Zheng, D. W. Luo, Y. Yuan, Z. Y. Wang, *J. Am. Ceram. Soc*., **98**, No. 10, 3231–3235 (2015).
10. Y. Y. Li, Y. R. Shi, G. Zhu, Q. S. Wu, *Inorg. Chem*., **53**, No. 14, 7668–7675 (2014).
11. X. Y. Huang, B. Li, H. Guo, *J. Alloys Compd*., **695**, 2773–2780 (2017).
12. L. Fan, X. Zhao, S. Zhang, Y. Ding, *J. Alloys Compd*., **579**, 432–437 (2013).
13. M. Xia, S. B. Zeng, J. Z. Wang, *China Light & Lighting*, **1**, 9–12 (2015).
14. A. Xie, X. M. Yuan, *New. Chem. Mater*., **36**, No. 12, 14–16 (2008).
15. S. H. Zhang, M. B. Zhou, J. F. Hu, B. Xie, *Int. Mater. Rev*., **23**, No. 9, 25–29 (2009).
16. N. N. Trac, H. V. Tuyen, V. X. Quang, *Phys. B*, **595**, 41237 (2020).
17. M. S. Huang, K. X. Zhang, Y. B. Zhang, Y. Z. Chen, *Rare Met. Cem. Carbides*, **40**, No. 1, 34–37 (2012).
18. X. Ding, Y. Xu, C. F. Guo, *Acta Phys. Sin*., **59**, No. 9, 6632–6636 (2010).
19. W. S. Song, Y. S. Kim, H. Yang, *Mater. Chem. Phys*., **117**, No. 2-3, 500–503 (2009).
20. Z. P. Yang, F. L. Zhang, X. N. Li, *Chin. J. Lumin*., **29**, No. 6, 941–944 (2008).
21. A. Lakshmanan, R. S. Bhaskar, P. C. Thomas, *Mater. Lett*., **64**, No. 16, 1809–1812 (2010).
22. R. Wang, J. Xu, C. Chen, *Chin. J. Lumin*., **32**, No. 10, 983–987 (2011).
23. H. H. Lin, S. Wu, Y. Y. Wu, *Bull. Chin. Ceram. Soc*., **32**, No. 1, 154–157 (2012).
24. T. H. Van, S. N. Manh, Q. V. Xuan, S. Bounyavong, *Luminescence*, **31**, No. 5, 1103–1108 (2015).
25. C. K. Chang, T. M. Chen, *Appl. Phys. Lett*., **91**, No. 8, 81902–81903 (2007).